Flow alignment in the helix uncoiling of sheared cholesteric liquid crystals

Alejandro D. Rey
Department of Chemical Engineering, McGill University, Montreal, Quebec, Canada H3A 2A7
(Received 11 September 1995)

This Brief Report analyzes the dependence of helix deformation modes on the flow alignment properties of sheared cholesteric liquid crystals. It is predicted that the helix of nonaligning cholesterics will not unwind. On the other hand, for flow-aligning cholesterics the helix will unwind only if the shear rate is larger than a pitch-dependent threshold.

PACS number(s): 64.70.Md, 47.20.Ft, 47.20.Hw, 47.50.+d

The objective of this Brief Report is to present a one-dimensional computational analysis that elucidates the fundamental role of flow alignment on the helix uncoiling of sheared cholesteric liquid crystals in finite geometries with free surfaces. We show that the shear flow-induced cholesteric-nematic transition (helix uncoiling) is predicted to occur (i) when the helix is oriented along the vorticity axes of the shear flow, (ii) at a reactive parameter [1] and pitch-dependent critical shear rate, (iii) only if the liquid crystal belongs to the shear flow-aligning [1–3] type. In addition, we show that the uncoiling of the cholesteric helix occurs through an increase of the cholesteric pitch beyond the sample size and by the divergence of the period of director rotations. Shear uncoiling of the cholesteric helix, originally oriented along the vorticity axis, with a fixed surface orientation was previously analyzed [4] by using minimization of a free energy, which may not be accurate for nonpotential flows, such as the simple shear flow [5] treated here.

A rheological property of nematic liquid crystals is their ability to orient close to the flow direction and in the shear plane when subjected to a shear flow. Nematics that display this property are known as flow aligning [3]. The flow-aligning angle is known as the Leslie angle θ_L and typically is less than 10°. Nematics that lack the ability to orient close to the flow direction are known as nonaligning. The parameter that determines flow alignment is known as the reactive parameter $\lambda=-\gamma_2/\gamma_1$, where γ_1 and γ_2 are the rotational and irrotational torque coefficients, respectively. Shear flow alignment may depend on the magnitude of the shear rate [6], temperature [1–3], or concentration [6]. The rheology of cholesterics is more complex than for nematics [7,8]. For the flow, geometry and helix orientation considered here the rheology is similar to that of nematics since layer instabilities and permeation [1,8] modes are absent. Flow alignment in cholesterics is again controlled by λ, but is now coupled to helix deformations and pitch and may result in the uncoiling of the helix.

Consider the shear start-up flow [5] of a cholesteric between two plates, of a finite width and with free surfaces along the vorticity direction. The flow direction is x, the shear gradient direction is y, the vorticity direction is z, and the shear plane is the x-y plane. At time $t=0$, a constant velocity field $\mathbf{v}(y)=(\dot{\gamma}y,0,0)$ is imposed on a cholesteric liquid crystal sample of width L (along "z"). The helix is oriented along the vorticity axis, and the planar director field is given by $\mathbf{n}(z,t)=(n_x(z,t),n_y(z,t),0)$. In the absence of flow the half-pitch [1] of the helix is P_e, which is the distance required for the director $\mathbf{n}$ to rotate by π radians. The flow domain along the z axis is $L=NP_e$, where N is the number of half-pitches. At $z=0$ and $z=L$ there are two free surfaces [1]. The director equation governing planar (i.e., $n_z=0$) cholesteric flows is given by

$$\frac{\partial \mathbf{n}}{\partial t}+(\mathbf{v}\cdot\nabla)\mathbf{n}-\mathbf{W}\cdot\mathbf{n}=\lambda[\mathbf{A}\cdot\mathbf{n}-(\mathbf{A}\cdot\mathbf{nn})\mathbf{n}]+K_2\{2(\mathbf{n}\cdot\nabla\times\mathbf{n})\times[\mathbf{n}(\mathbf{n}\cdot\nabla\times\mathbf{n})-\nabla\times\mathbf{n}]+\mathbf{n}\times\nabla(\mathbf{n}\cdot\nabla\times\mathbf{n})\}/\gamma_1, \tag{1}$$

where $\mathbf{W}(\mathbf{A})$ is the antisymmetric (symmetric) part of the velocity gradient tensor ($\nabla\mathbf{v}$), λ is the reactive parameter, K_2 is the twist elastic modulus, and γ_1 is the rotational viscosity. With the adopted director field, Eq. (1) is a two component (n_x,n_y) nonlinear reaction-diffusion system [9]. We introduce a phase $\theta(y,t)$, here denoted as orientation and measured anticlockwise from the flow direction (x) in units of radians. In terms of θ, the planar director field is $\mathbf{n}=(\cos\theta,\sin\theta,0)$, and Eq. (1) becomes

$$\frac{\partial\theta}{\partial t^*}+E(1-\lambda\cos 2\theta)-\frac{\partial^2\theta}{\partial z^{*2}}=0, \tag{2}$$

where $t^*=tK_{22}/\gamma_1L^2$ is the dimensionless time, $z^*=zL$ the dimensionless distance, and $E=\dot{\gamma}\gamma_1L^2/(2K_{22})$ is the Ericksen number. The auxiliary conditions are

$$t=0,\quad \theta=N\pi z^*; \tag{3a}$$

$$z^*=0 \text{ and } z^*=1,\quad \frac{\partial\theta}{\partial z^*}=N\pi, \tag{3b}$$

which ensures the existence of a stable helix both prior to and after cassation of flow, and free surfaces at $z^*=0$ and $z^*=1$. Here we consider a right-handed helix ($\partial\theta/\partial z^*>0$). Solutions to (2) and (3) were obtained using the Galerkin finite element method with 200 linear elements. Analytical solutions to Eq. (2) in the absence of diffusion ($K_2=0$) are given by [10]

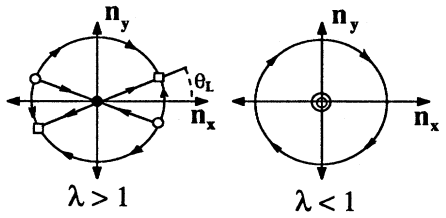

FIG. 1. Phase plane trajectories and critical points. See text.

$$\lambda > 1: \quad \theta_L = \frac{1}{2}\cos^{-1}\left[\frac{1}{\lambda}\right] \pm n\pi; \tag{4a}$$

$$\lambda < 1: \quad \tan\theta = -\left(\frac{1-\lambda}{1+\lambda}\right)^{1/2} \tan\left\{\frac{\dot{\gamma}}{2}\sqrt{1-\lambda^2}\,t\right\}, \tag{4b}$$

where n is an integer, and where $\theta(t=0)=0$ in (4b). Figure 1 shows the phase plane trajectories and critical points for $\lambda>1$ and $\lambda<1$, respectively. For $\lambda>1$ the trajectory is the unit circle connecting two stable nodes (squares) with two unstable sources (circles), joined with a saddle (dot) at the origin. For $\lambda<1$ the trajectory is the unit circle with a center (two circles) at the origin. From Fig. 1 it follows that if $\lambda>1$ sufficiently strong flows ($E>E_c$) uncoil the helix by adopting the uniform orientation given by (4a), while if $\lambda<1$ the helix cannot be uncoiled since no stationary spatially homogeneous solution exists; E_c is the critical value for the helix uncoiling and is a function of λ and P_e. Figure 2 shows a phase diagram in terms of λ and E, for $N=3$. There are three phase fields: for $0<\lambda<1$ the solutions are right traveling waves on the rotating cholesteric helix; for $\lambda>1$ and sufficiently small E ($E<E_c$) the solutions are also traveling waves on the rotating cholesteric helix; for $\lambda<1$ and sufficiently large E ($E>E_c$) the solutions are stationary, and the helix is uncoiled into a nematic state. In Fig. 2 the stars are numerical solutions and the diverging curve (thin full line) represents the shear flow-induced cholesteric-nematic transition. A balance between elastic and viscous torques that captures the helix uncoiling is given by [11]

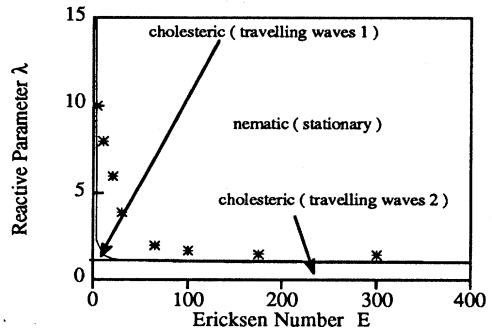

FIG. 2. Computed phase diagram in terms of λ and E. The stars represent computed values of (E,λ) at which the helix uncoils, the orientation is stationary and of nematic symmetry. See text.

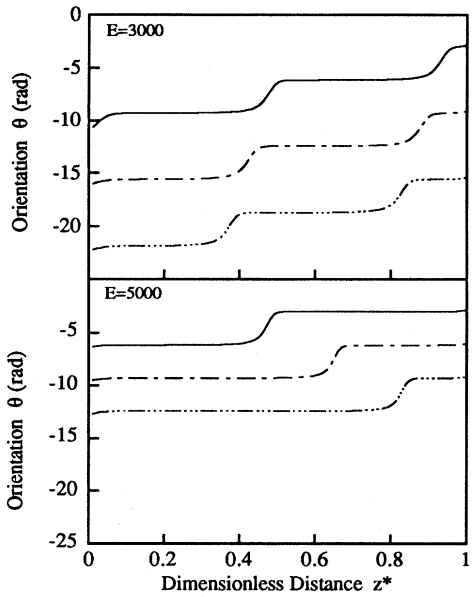

FIG. 3. Orientation $\theta(z^*,t)$ as a function of dimensionless distance z^* for $E=3000$ (top) and $E=5000$ (bottom) at three different times; $\lambda=1.04$. The dimensionless times are t^*: 0.02 (full line), 0.03 (dashed line), and 0.04 (dashed-dotted line). See text.

$$\frac{K_2}{P_e^2} = \gamma_1(\lambda-1)\dot{\gamma}, \quad \lambda>1, \tag{5}$$

which when written in terms of the critical Ericksen number E_c gives

$$E_c = \frac{N^2}{2}(\lambda-1)^{-1} \tag{6}$$

in agreement with the numerical results. Next we show representative numerical results that characterize the three phase fields and the helix uncoiling. Cases of practical interest are found when $\lambda \approx 1$ [12]. All results are for $N=3$.

(a) Weak shearing of flow aligning cholesterics ($E<E_c, \lambda>1$). In this region (lower left region of Fig. 2) the helix is distorted, the pitch increases, the helix rotates clockwise, and the solutions are right traveling waves, distinguished for convenience by the integer 1. Helix distortions, pitch, and rotation period increase with increasing E. Here we show solutions for $\lambda=1.04$, corresponding to PAA, which at these conditions is a flow aligning nematic material [1]. For this λ we find that $E_c=5440$. Figure 3 shows the orientation as a function of distance z^* for three times and $E=3000$ (top) and $E=5000$ (bottom). At any given time the orientation is stairlike, denoting a distorted helix; the orientation of the steps are given by (4a) and are connected with their neighbors through twist inversion walls [1]. The pitch at $E=3000$ is larger than at $E=0$. At $E=5000$ the pitch is longer than the sample width. Comparing the vertical distance between two successive profiles in the top and bottom figures shows that as $E>E_c=5440$, the director rotation period at any z^* increases. The pitch increases with increasing E because the flow-aligning strength along θ_L increases,

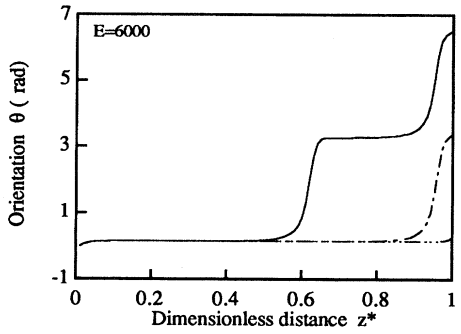

FIG. 4. Flow aligning case. Orientation $\theta(z^*,t)$ as a function of dimensionless distance z^*, for three increasing times and $E=6000>E_c=5440$; $\lambda=1.04$. See text.

causing the director to stay longer and longer along θ_L, and because boundary rotations are unhindered.

(b) Strong shearing of flow-aligning cholesterics ($E>E_c,\lambda>1$). In this region (upper right region of Fig. 2) the helix has been uncoiled and the solutions are stationary. Figure 4 shows the orientation as a function of distance z^*, for three increasing times and $E=6000>E_c$. The initial traveling front leads to a stationary orientation, given by (4a) except in the two thin boundary layers. For $E>E_c$, flow dominates over helix elasticity and a practically uniform nematic flow alignment is attained.

(c) Shear uncoiling of the cholesteric helix ($E\approx E_c,\lambda>1$). The transition region corresponding to the shear uncoiling of the helix at $E=E_c(\lambda)$ is shown by the stars in Fig. 2. As $E\rightarrow E_c$ the pitch increases, and as the flow strength increases each director rotation period increases, spending longer times aligned along θ_L. At $E=E_c$ the pitch is already longer than the sample size and the period of director rotational motion diverges, resulting in a stationary nematic state. Figure 5 shows the dimensionless period T^* of the director's rotational motion at $z^*=0.5$ as a function of E, for $\lambda=1.042$, where T^* is the dimensionless time required for the director to rotate by π radians. The divergence of the period (Fig. 5) at $E_c=5440$ is indicated by the vertical full line. Figure 6 shows the orientation θ as a function of time, for $z^*=0.5,\lambda=1.04$, and three increasing E. For $E<E_c$ the director rotates anticlockwise with a stairlike profile, whose

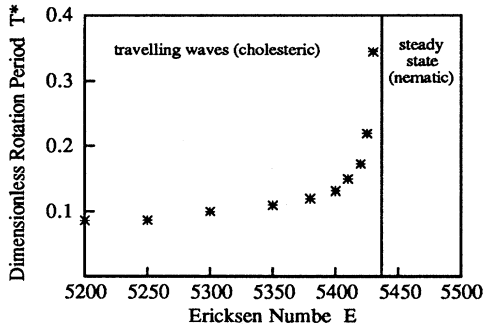

FIG. 5. Dimensionless period T^* of the director's rotational motion at $z^*=0.5$ as a function of E, for $\lambda=1.04$. See text.

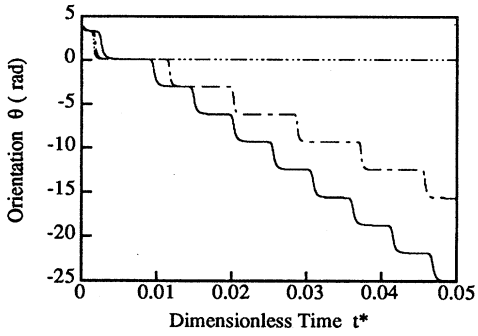

FIG. 6. Flow aligning case. Orientation $\theta(z^*,t)$ as a function of dimensionless time t^*, for $z^*=0.5$, $\lambda=1.04$, and three increasing E. $E=3000$ (full line), $E=5000$ (dashed line), and $E=6000$ (dashed-dotted line). See text.

steps increase with increasing E (compare the full and dashed lines). For $E>E_c$ the director attains a steady value given by (4a).

(d) Shearing of nonaligning cholesterics ($E>E_c,0<\lambda<1$). In this parametric region (bottom region of Fig. 2) the helix is distorted, the pitch decreases, the helix rotates clockwise, and the orientation θ solutions are traveling waves, distinguished for convenience by the integer 2. The rotation period decreases with increasing E, in stark contrast to case (a), and as expected from (4b). At large E the pitch remains close to the equilibrium value. The different sensitivity of the traveling wave solutions for $\lambda>1$ and $\lambda<1$ with respect to E is identified by the integers 1 and 2, respectively (see Fig. 2). Without loss of generality we show solutions for $\lambda=0.99$. Figure 7 shows the orientation as a function of distance z^* for three times and $E=6000$. At any given time the orientation is stairlike, denoting a distorted helix; the steps are located at $n\pi$ ($n=0,1,\ldots$), and are connected by twist inversion walls [1]. The pitch at $E=6000$ is slightly shorter than at $E=0$. Figure 8 shows the orientation θ as a function of time, for $z^*=0.5,\lambda=0.99$, and four increasing E. As E increases the director's rotation become more uniform (i.e., shorter steps) and the period decreases, as shown by Eq. (4b). For $\lambda<1$ the helix can never be uncoiled, in agreement with Fig. 1 (right) and Eq. (4b), because there

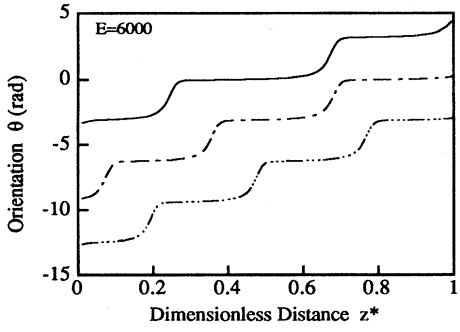

FIG. 7. Flow nonaligning case. Orientation $\theta(z^*,t)$ as a function of dimensionless distance z^* for $E=6000$ at three different times; $\lambda=0.99$. The dimensionless times are t^*: 0.0025 (full line), 0.005 (dashed line), and 0.0075 (dashed-dotted line). See text.

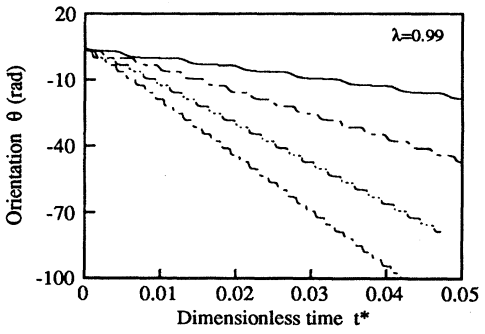

FIG. 8. Flow nonaligning case. Orientation $\theta(z^*,t)$ as a function of dimensionless time t^*, for $z^*=0.5$, $\lambda=0.99$, and four increasing E. $E=1000$ (full line), $E=3000$ (long dashed line), $E=6000$ (dashed-dotted line), and $E=9000$ (short dashed line). See text.

is no single preferred alignment direction.

In conclusion, we have shown that the phase diagram for a sheared cholesteric liquid crystal with the helix along the vorticity axis is given by the Ericksen number E and the reactive parameter λ. If the material is of the nonaligning type, helix uncoiling does not occur in this geometry. If the material is flow aligning and the flow is sufficiently strong, the helix uncoils and the orientation is stationary, practically uniform, and of nematic symmetry. The traveling wave mode 1 that leads to the helix uncoiling is an example of multisoliton solutions to liquid crystal shear flows [13].

In closing, we mention that, although the initial helix orientation was not a parameter in this study, a number of significant conclusions can be reached from the present results and previously published results. If the reactive parameter of a cholesteric is less than 1, the helix will not uncoil regardless of its initial orientation. This follows from the present results and from extensive numerical studies of liquid crystal flows [2,3], which show that nonaligning nematic liquid crystals adopt the cholesteric twisted structure with the helix oriented along the velocity gradient of the shear flow. It then follows from [2,3] that shearing a nonaligning cholesteric with the helix oriented along the velocity gradient will not result in the uncoiling of the helix nor in the formation of a nonequilibrium nematic phase. Extensive experimental work on cholesteric shear rheology [14] shows that shearing cholesterics in the Grandjean texture will never result in the nematic ordering. On the other hand, shearing a cholesteric initially aligned along the velocity direction will result in permeative flows [1] and again will not result in the helix uncoiling. Thus we reach the significant conclusion that shear uncoiling of the cholesteric helix into a nematic state is a highly unlikely transformation that may only occur under the flow and material conditions identified in this Brief Report.

This work is supported by the Natural Science and Engineering Research Council of Canada.

[1] P. G. de Gennes and J. Prost, *The Physics of Liquid Crystals*, 2nd ed. (Oxford University Press, Oxford, 1993).
[2] W. H. Han and A. D. Rey, Phys. Rev. E **49**, 597 (1994).
[3] W. H. Han and A. D. Rey, Phys. Rev. E **50**, 1688 (1994).
[4] G. Derfel, Mol. Cryst. Liq. Cryst. Lett. **92**, 41 (1983).
[5] R. G. Larson, *Constitutive Equations for Polymer Melts and Solutions* (Butterworths, Boston, 1988).
[6] G. Marrucci, in *Liquid Crystallinity in Polymers*, edited by A. Ciferri (VCH, New York, 1991), p. 395.
[7] U. D. Kini, J. Phys. **40**, C3-62 (1979).
[8] N. Sacaramuzza and V. Carbone, in *Physics of Liquid Crystalline Materials*, edited by I-C Khoo and F. Simoni (Gordon and Breach, Philadelphia, 1988), p. 517.
[9] J. D. Murray, *Mathematical Biology*, 2nd ed. (Springer-Verlag, New York, 1993), p. 311.
[10] J. L. Ericksen, Kolloid Z. **5**, 117 (1960).
[11] I. Janossy, Ann. Phys. **2**, 345 (1979).
[12] S. D. Lee and R. B. Meyer, in *Liquid Crystallinity in Polymers*, edited by A. Ciferri (VCH, New York, 1991), p. 343.
[13] L. Lam, in *Solitons in Liquid Crystals*, edited by L. Lam and J. Prost (Springer Verlag, New York, 1992), pp. 51–107.
[14] J. M. Pochan, in *Liquid Crystals*, edited by F. D. Saeva (Dekker, New York, 1979), pp. 275–304.